Electroweak radiative corrections for polarized Møller scattering at the future 11 GeV JLab experiment

Aleksandrs Aleksejevs[*]

Memorial University, Corner Brook, Canada, A2H 6P9

Svetlana Barkanova[†]

Acadia University, Wolfville, Canada, B4P 2B2

Alexander Ilyichev[‡]

National Center of Particle and High Energy Physics, 220040 Minsk, Belarus

Vladimir Zykunov[§]

Belarussian State University of Transport, 246653 Gomel, Belarus

We perform updated and detailed calculations of the complete next-to-leading order set of electroweak radiative corrections to parity-violating $e^- e^- \to e^- e^- (\gamma)$ scattering asymmetries at energies relevant for the ultraprecise Møller experiment to be performed at JLab. Our numerical results are presented for a range of experimental cuts and the relative importance of various contributions is analyzed. We also provide very compact expressions analytically free from nonphysical parameters and show them to be valid for fast, yet accurate estimations.

I. INTRODUCTION

There are several reasons why polarized Møller scattering has attracted so much interest from both the experimental and theoretical communities. The scattering of two identical polarized fermions has been used in many laboratories for the high-precision determination of the electron-beam polarization, including SLC in [1], the E-143 [2] and E-154 [3] experiments at SLAC, and several experiments at JLab [4] and MIT-Bates [5]. A Møller polarimeter may also be of use in future experiments planned at ILC [6]. The E-158 experiment at SLAC [7], which studied Møller scattering of 45- to 48-GeV polarized electrons on the unpolarized electrons of a hydrogen target, allowed one of the most important parameters in the standard model—the sine of the Weinberg angle—to be determined with unprecedented accuracy. The next-generation experiment at 11 GeV soon to begin at JLab will offer a new level of sensitivity and measure the parity-violating asymmetry in the scattering of longitudinally polarized electrons off unpolarized electrons to a precision of 0.73 ppb. That would allow a measurement of the weak charge of the electron to a fractional accuracy of 2.3% and a determination of the weak mixing angle with an uncertainty of $\pm 0.00026(\text{stat}) \pm 0.00013(\text{syst})$ [8].

Since $e^- e^- \to e^- e^- (\gamma)$ scattering is a very clean process with a well-known initial energy and extremely

suppressed backgrounds, any inconsistency with the standard model will signal new physics. Møller scattering experiments can provide indirect access to physics at multi-TeV scales and play an important complementary role to the LHC research program [9].

Obviously, before we can extract reliable information from the experimental data, it is necessary to take into account higher order effects. These are the processes which are more complicated than the process being studied, but which are indistinguishable from it experimentally. This procedure of the inclusion of radiative corrections is an indispensable part of any modern experiment, but will be of the most paramount importance for the ultraprecise measurement of the weak mixing angle via 11 GeV Møller scattering planned at JLab.

One of the earliest studies on electroweak radiative corrections (EWC) to the observables of Møller scattering was done by Czarnecki and Marciano [10]. According to their calculations for the asymmetry in the E-158 kinematical region, the EWC reduce the tree level prediction by $40\% \pm 3\%$. A similar value for the asymmetry was obtained in the study of Denner and Pozzorini [11], where radiative corrections in polarized Møller scattering were examined at arbitrary, including high, energies. It is worth noticing that these two studies used different renormalization schemes: [10] employed the modified minimal-subtraction scheme and [11] used the on-shell renormalization. However, the authors of [10,11] did not take into account all radiative contributions consistently. For example, they completely disregarded the hard photon bremsstrahlung (HPB) contribution assuming that it was

---

[*]aaleksejevs@swgc.mun.ca
[†]svetlana.barkanova@acadiau.ca
[‡]ily@hep.by
[§]vladimir.zykunov@cern.ch

small. The first computation of the HPB contributions with realistic experimental cuts was done by Petriello [12] who studied a total set of the lowest-order EWC under the kinematical conditions of the E-158 experiment. He clearly showed that experimental cuts play a significant role. Later works [13–15] dedicated to the EWC for the E-158 experiment, which employed a covariant method for extracting of infrared divergences [16], showed a good agreement with [10] for the bulk of the weak-interaction contributions and proved that the effect of HPB was below the experimental error of E-158.

Electromagnetic radiative corrections, which dominate the weak-interaction effects at the energies of E-158, and their effect on the measurement of beam polarization in a Møller polarimeter were assessed in [17]. A different calculation of these electromagnetic corrections was undertaken in [18], where attention was primarily given to the effect of experimental cuts on the inelasticity and, accordingly, proving the need for taking into account HPB in experiments of this kind. A Monte Carlo generator that makes it possible to simulate radiative events in a Møller process at moderate energies with the aim of determining beam polarization was developed in [19].

Finally, an attempt to calculate the HPB contribution for the Møller process at high energies was made in paper [20]. A feature specific to this calculation, as well as to the calculations in [11,12], was the use of a parameter ω that separates regions of soft and hard photons. As a result, the Monte Carlo integration technique permitted the development of a code which made it possible to take into account radiative corrections in the case of arbitrary cuts imposed on the detection of electrons.

Although obviously significant theoretical effort has already been dedicated to this task, we can see at least three major reasons for addressing EWC to Møller scattering yet again. First, since the new experiment at Jlab will provide more precise information than, for example, E-158, the theoretical predictions for this ultraprecise measurement must be made with a full treatment of one-loop radiative corrections and at least leading two-loop corrections. In this work, we calculated the full set of the one-loop corrections both numerically with no simplifications using FEYNARTS and FORMCALC [21] as the base languages and analytically in a compact form useful for fast estimations. This way, we can control the accuracy of asymptotic approximations at the one-loop level very well now, so we hope that the same idea will help us to control the accuracy as we calculate leading corrections at two-loop level in the near future. The next major goal of the presented paper is to get EWC in a form which is analytically free from nonphysical parameters. And, finally, we believe that the complexity of the problem demands a tuned comparison with different calculation schemes. This will be our next task.

The rest of the paper is organized as follows. The basic notations as well as the lowest-order (Born) contribution to

Møller scattering are presented in Sec. II. The contribution from a full set of additional virtual particles (such as self-energies, vertices, and boxes) is described in Sec. III. The real photon emission and its separation into hard and soft parts as well as cancellation of the infrared divergences together with the unphysical parameters can be found in Sec. IV. The numerical analysis is presented in Sec. V and Appendix C.

II. BORN CROSS SECTION: BASIC NOTATION AND CONVENTIONS

In the standard model, the Born cross section for Møller scattering

$$e^-(k_1, \xi) + e^-(p_1, \eta) \rightarrow e^-(k_2) + e^-(p_2) \qquad (1)$$

can be represented in the form

$$\sigma^0 = \frac{\pi\alpha^2}{s} \sum_{i,j=\gamma,Z} [\lambda_-^{i,j}(u^2 D^{it} D^{jt} + t^2 D^{iu} D^{ju})$$
$$+ \lambda_+^{i,j} s^2 (D^{it} + D^{iu})(D^{jt} + D^{ju})], \qquad (2)$$

with $\sigma \equiv d\sigma/d\cos\theta$, where θ is the scattering angle of the detected electron with 4-momentum k_2 in the center of mass system of the initial electrons and the 4-momenta of initial (k_1 and p_1) and final (k_2 and p_2) electrons (see Fig. 1) generate a standard set of Mandelstam variables,

$$s = (k_1 + p_1)^2, \qquad t = (k_1 - k_2)^2, \qquad u = (k_2 - p_1)^2, \qquad (3)$$

while the electron polarization vectors ξ and η have the form [22]:

$$\xi \approx \frac{k_1}{m} - \frac{2m}{s} p_1, \qquad \eta \approx \frac{2m}{s} k_1 - \frac{p_1}{m}. \qquad (4)$$

It should also be noted that the electron mass m is disregarded wherever possible, in particular, if $m^2 \ll s$, $-t$, $-u$.

A useful structure in the present study is

$$D^{il} = \frac{1}{l - m_i^2} (i = \gamma, Z; l = t, u), \qquad (5)$$

which depends on the Z-boson mass m_Z and on the photon mass m_γ. The photon mass is set to zero everywhere with
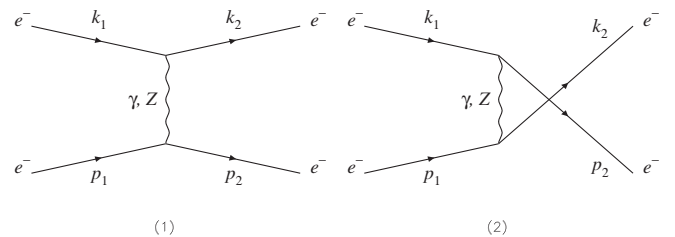

FIG. 1.   Diagrams describing nonradiative Møller scattering in the (1) t and (2) u channels.

the exception of specially indicated cases where the photon mass is taken to be an infinitesimal parameter that regularizes an infrared divergence. Another set of useful functions is

$$\lambda_{\pm}^{i,k} = \lambda_{1B}^{i,k}\lambda_{1T}^{i,k} \pm \lambda_{2B}^{i,k}\lambda_{2T}^{i,k}, \tag{6}$$

which are combinations of coupling constants and $p_{B(T)}$, where $p_{B(T)}$ are the degrees of polarization of electrons with 4-momentum k_1 (p_1). Specifically, they are given by

$$\lambda_{1B(T)}^{i,j} = \lambda_V^{i,j} - p_{B(T)}\lambda_A^{i,j}, \qquad \lambda_{2B(T)}^{i,j} = \lambda_A^{i,j} - p_{B(T)}\lambda_V^{i,j},$$
$$\lambda_V^{i,j} = v^i v^j + a^i a^j, \qquad \lambda_A^{i,j} = v^i a^j + a^i v^j, \tag{7}$$

where

$$v^\gamma = 1, \qquad\qquad a^\gamma = 0,$$
$$v^Z = (I_e^3 + 2s_W^2)/(2s_W c_W), \qquad a^Z = I_e^3/(2s_W c_W). \tag{8}$$

It should be recalled that $I_e^3 = -1/2$ and $s_W(c_W)$ is the sine (cosine) of the Weinberg angle expressed in terms of the Z- and W-boson masses according to the rules of the standard model:

$$c_W = m_W/m_Z, \qquad s_W = \sqrt{1 - c_W^2}. \tag{9}$$

The electron polarization degrees $p_{B(T)}$ in the cross sections are labeled here as follows: the subscripts L and R on the cross sections correspond to $p_{B(T)} = -1$ and $p_{B(T)} = +1$, where the first subscript indicates the degree of polarization for the 4-momentum k_1, while the second one indicates the degree of polarization for the 4-momentum p_1. By combining the degrees of electron-beam polarizations, we can obtain four measurable cross sections, but, by virtue of the rotational invariance, the two of them will be identical: $\sigma_{LR} = \sigma_{RL}$. From the three cross sections we can construct three independent asymmetries [23] (which are very close at large scattering angles), and the two of them (mainly A_1) are the main subject of our investigation:

$$A_1 = \frac{\sigma_{LL} + \sigma_{LR} - \sigma_{RL} - \sigma_{RR}}{\sigma_{LL} + \sigma_{LR} + \sigma_{RL} + \sigma_{RR}} = \frac{\sigma_{LL} - \sigma_{RR}}{\sigma_{LL} + 2\sigma_{LR} + \sigma_{RR}}, \tag{10}$$

$$A_2 = \frac{\sigma_{LL} - \sigma_{RR}}{\sigma_{LL} + \sigma_{RR}}. \tag{11}$$

All of the asymmetries are proportional to the combination $1 - 4s_W^2$ (by virtue of the proportionality of the cross-section difference $\sigma_{LL} - \sigma_{RR}$) and are therefore highly sensitive to small changes in s_W. This is precisely the reason why the asymmetry A_1, which, at moderately low energies, is given by

$$A_1 = \frac{s}{2m_W^2} \frac{y(1-y)}{1 + y^4 + (1-y)^4} \frac{1 - 4s_W^2}{s_W^2}, \qquad y = -t/s, \tag{12}$$

was used as the observable in E-158 and will be measured in the future experiment at JLab with 11 GeV electrons.

In addition to the fact that the asymmetry A_1 is a parity-violating observable, this asymmetry has yet another remarkable property based on its structure: it only involves combinations $\sigma_{LL} + \sigma_{LR}$ and $\sigma_{RL} + \sigma_{RR}$, which can be interpreted as the cross sections for the scattering of electrons having the polarizations of $p_B = -1$ and $p_B = +1$ on unpolarized electrons. Frequently, A_1 is said to be a single-polarization asymmetry, in contrast to the asymmetry constructed as

$$A_{LR} = \frac{\sigma_{LR} - \sigma_{LL}}{\sigma_{LR} + \sigma_{LL}}, \tag{13}$$

which consists of the cross sections for the scattering of electrons having different polarizations. The latter asymmetry, which conserves parity, is the most important observable in determining the electron-beam polarization with the aid of a Møller polarimeter.

III. EWC: CONTRIBUTION OF ADDITIONAL VIRTUAL PARTICLES

A. Boson self-energies

The contribution of virtual particles (V contribution) to the observables of Møller scattering is described by three classes of diagrams (see Fig. 2): boson self-energies (BSE), vertex functions, and two-boson exchange (boxes). In the on-shell renormalization schemes which we use here there are no contributions from the electron self-energies.

The corresponding cross section is given by

$$\sigma^V = \sigma^{\mathrm{BSE}} + \sigma^{\mathrm{Ver}} + \sigma^{\mathrm{Box}}, \tag{14}$$

where the first term corresponds to the contributions of the boson self-energies, the second term represents the vertex diagrams, and the third term stands for the diagrams of two-boson exchange.
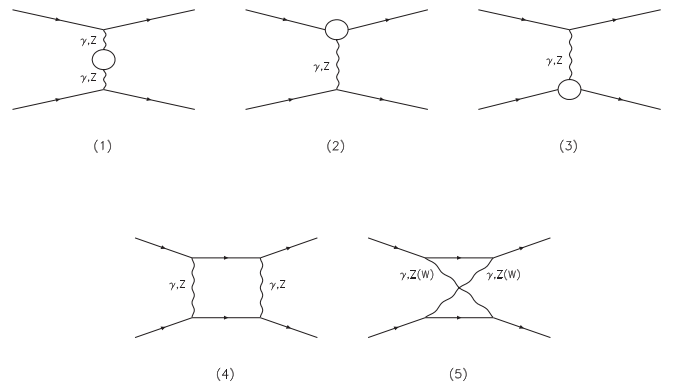

FIG. 2. One-loop t-channel diagrams for the Møller process. The circles represent the contributions of self-energies and vertex functions. The u-channel diagrams are obtained via the interchange $k_2 \leftrightarrow p_2$.

The contributions of the photon and Z-boson self-energies are shown symbolically in Fig. 2(1). They do not involve infrared divergences and have the following form:

$$\sigma^{\text{BSE}} = \frac{\pi\alpha^2}{s} \sum_{l=1}^{8} M_l^S + (t \leftrightarrow u), \tag{15}$$

where M_l^S are expressed in terms of the propagators and functions $M_{\text{ev,od}}$

$$M_{\text{ev}}^{ijkl} = 2(s^2 + u^2)\lambda_{1B}^{ij}\lambda_{1T}^{kl} + 2(s^2 - u^2)\lambda_{2B}^{ij}\lambda_{2T}^{kl},$$
$$M_{\text{od}}^{ijkl} = -2s^2(\lambda_{1B}^{ij}\lambda_{1T}^{kl} + \lambda_{2B}^{ij}\lambda_{2T}^{kl}), \tag{16}$$

are defined as

$$M_1^S = D^{\gamma t}D_S^{\gamma Zt}(M_{\text{ev}}^{\gamma\gamma Z\gamma} + M_{\text{ev}}^{Z\gamma\gamma\gamma}),$$
$$M_2^S = -D^{\gamma u}D_S^{\gamma Zt}(M_{\text{od}}^{\gamma\gamma Z\gamma} + M_{\text{od}}^{Z\gamma\gamma\gamma}),$$
$$M_3^S = D^{Zt}D_S^{\gamma Zt}(M_{\text{ev}}^{\gamma ZZZ} + M_{\text{ev}}^{ZZ\gamma Z}),$$
$$M_4^S = -D^{Zu}D_S^{\gamma Zt}(M_{\text{od}}^{\gamma ZZZ} + M_{\text{od}}^{ZZ\gamma Z}),$$
$$M_5^S = D^{\gamma t}(D_S^{\gamma\gamma t}M_{\text{ev}}^{\gamma\gamma\gamma\gamma} + D_S^{ZZt}M_{\text{ev}}^{Z\gamma Z\gamma}), \tag{17}$$
$$M_6^S = -D^{\gamma u}(D_S^{\gamma\gamma t}M_{\text{od}}^{\gamma\gamma\gamma\gamma} + D_S^{ZZt}M_{\text{od}}^{Z\gamma Z\gamma}),$$
$$M_7^S = D^{Zt}(D_S^{\gamma\gamma t}M_{\text{ev}}^{\gamma Z\gamma Z} + D_S^{ZZt}M_{\text{ev}}^{ZZZZ}),$$
$$M_8^S = -D^{Zu}(D_S^{\gamma\gamma t}M_{\text{od}}^{\gamma Z\gamma Z} + D_S^{ZZt}M_{\text{od}}^{ZZZZ}).$$

Here,

$$D_S^{ijl} = -D^{il}\hat{\Sigma}_T^{ij}(l)D^{jl}, \tag{18}$$

with $\hat{\Sigma}_T^{ij}(l)$ being the transverse part of the renormalized photon, Z boson and γZ self-energies. The longitudinal parts of the boson self-energy make contributions that are proportional to the ratios m^2/t and m^2/u so they are very small and are not considered here.

B. Vertices

In order to calculate the electron vertex corrections (2nd and 3rd diagrams in Fig. 2), we use the form factors $\delta F_{V,A}^{je}$ in the manner of paper [24]. Replacing the coupling constants v^j, a^j with these form factors (for example, $v^{\gamma(Z)} \rightarrow \delta F_V^{\gamma(Z)e}$, $a^{\gamma(Z)} \rightarrow \delta F_A^{\gamma(Z)e}$) in the corresponding terms of the Born functions $M_{\text{ev,od}}$, we obtain a vertex part of the cross sections in the form

$$\sigma^{\text{Ver}} = \frac{\pi\alpha^2}{s} \sum_{l=1}^{4} M_l^V + (t \leftrightarrow u), \tag{19}$$

where

$$M_1^V = D^{\gamma t}(D^{\gamma t}(M_{\text{ev}}^{F^\gamma\gamma\gamma\gamma} + M_{\text{ev}}^{\gamma\gamma F^\gamma\gamma}) - D^{\gamma u}(M_{\text{od}}^{F^\gamma\gamma\gamma\gamma} + M_{\text{od}}^{\gamma\gamma F^\gamma\gamma})),$$
$$M_2^V = D^{\gamma t}(D^{Zt}(M_{\text{ev}}^{F^\gamma Z\gamma Z} + M_{\text{ev}}^{\gamma ZF^\gamma Z}) - D^{Zu}(M_{\text{od}}^{F^\gamma Z\gamma Z} + M_{\text{od}}^{\gamma ZF^\gamma Z})),$$
$$M_3^V = D^{Zt}(D^{\gamma t}(M_{\text{ev}}^{F^Z\gamma Z\gamma} + M_{\text{ev}}^{Z\gamma F^Z\gamma}) - D^{\gamma u}(M_{\text{od}}^{F^Z\gamma Z\gamma} + M_{\text{od}}^{Z\gamma F^Z\gamma})), \tag{20}$$
$$M_4^V = D^{Zt}(D^{Zt}(M_{\text{ev}}^{F^Z ZZZ} + M_{\text{ev}}^{ZZF^Z Z}) - D^{Zu}(M_{\text{od}}^{F^Z ZZZ} + M_{\text{od}}^{ZZF^Z Z})),$$

and

$$\lambda_V^{Fi,j} = \delta F_V^i v^j + \delta F_A^i a^j, \qquad \lambda_A^{Fi,j} = \delta F_V^i a^j + \delta F_A^i v^j. \tag{21}$$

For the virtual photon exchange [$i = \gamma$ in Eq. (5)], the vertices look like

$$\delta F_V^\gamma = \frac{\alpha}{4\pi}\left[\Lambda_1 + ((v^Z)^2 + (a^Z)^2)\Lambda_2(m_Z) + \frac{3}{4s_W^2}\Lambda_3(m_W)\right], \tag{22}$$

$$\delta F_A^\gamma = \frac{\alpha}{4\pi}\left[2v^Z a^Z \Lambda_2(m_Z) + \frac{3}{4s_W^2}\Lambda_3(m_W)\right], \tag{23}$$

and for the virtual Z-boson exchange [$i = Z$ in Eq. (5)] we have the form

$$\delta F_V^Z = \frac{\alpha}{4\pi}\left[v^Z\Lambda_1 + v^Z((v^Z)^2 + 3(a^Z)^2)\Lambda_2(m_Z) + \frac{1}{8s_W^3 c_W}\Lambda_2(m_W) - \frac{3c_W}{4s_W^3}\Lambda_3(m_W)\right], \tag{24}$$

$$\delta F_A^Z = \frac{\alpha}{4\pi}\left[a^Z\Lambda_1 + a^Z(3(v^Z)^2 + (a^Z)^2)\Lambda_2(m_Z) + \frac{1}{8s_W^3 c_W}\Lambda_2(m_W) - \frac{3c_W}{4s_W^3}\Lambda_3(m_W)\right]. \tag{25}$$

Function Λ_1 is the contribution of triangle diagrams with an additional photon, Λ_2 refers to the triangle diagrams with an additional massive boson—Z or W, and Λ_3 corresponds to the triangle diagrams with 3-boson vertices—$WW\gamma$ or WWZ. We denote the vertices with an additional photon as light vertices (LV) and the vertices with an additional massive boson as heavy vertices (HV). The LV

terms are proportional to the function Λ_1, and the HV terms are proportional to the combinations of functions Λ_2 and Λ_3 as it is evident from Eqs. (22)–(25).

The contributions of separate HV, γZ, and ZZ self-energies strongly depend on the details of the renormalization scheme and for a proper account of EWC they should be taken in numerical analysis as one gauge independent set. For that purpose we used the on-shell renormalization scheme from Ref. [25]. It is of crucial importance to raise a question of dependence of EWC on details of different renormalization schemes and this will be addressed in our following paper.

Next, we represent the vertex contribution as the sum of infrared (IR) divergent and finite parts using the identical transformation

$$\sigma^{\mathrm{Ver}} = (\sigma^{\mathrm{Ver}} - \sigma^{\mathrm{Ver}}(\lambda^2 \to s)) + \sigma^{\mathrm{Ver}}(\lambda^2 \to s)$$
$$= \sigma_{\mathrm{IR}}^{\mathrm{Ver}} + \sigma^{\mathrm{Ver}}(\lambda^2 \to s), \tag{26}$$

where λ is the photon mass which regularizes the infrared divergence. Then the IR part of the vertex cross section will look like

$$\sigma_{\mathrm{IR}}^{\mathrm{Ver}} = \frac{\alpha^3}{2s}\Lambda_1^{\mathrm{IR}}\sum_{l=1}^{4}M_l^0 + (t \leftrightarrow u), \tag{27}$$

where

$$\Lambda_1^{\mathrm{IR}} = \Lambda_1 - \Lambda_1(\lambda^2 \to s) = -2\log\frac{s}{\lambda^2}\log\frac{-t}{em^2}, \tag{28}$$

e is the base of the natural logarithm, and

$$\begin{aligned}
M_1^0 &= D^{\gamma t}(D^{\gamma t}M_{\mathrm{ev}}^{\gamma\gamma\gamma\gamma} - D^{\gamma u}M_{\mathrm{od}}^{\gamma\gamma\gamma\gamma}),\\
M_2^0 &= D^{\gamma t}(D^{Zt}M_{\mathrm{ev}}^{\gamma Z\gamma Z} - D^{Zu}M_{\mathrm{od}}^{\gamma Z\gamma Z}),\\
M_3^0 &= D^{Zt}(D^{\gamma t}M_{\mathrm{ev}}^{Z\gamma Z\gamma} - D^{\gamma u}M_{\mathrm{od}}^{Z\gamma Z\gamma}),\\
M_4^0 &= D^{Zt}(D^{Zt}M_{\mathrm{ev}}^{ZZZZ} - D^{Zu}M_{\mathrm{od}}^{ZZZZ}).
\end{aligned} \tag{29}$$

It is worth noticing that since the Born cross section can be presented as

$$\sigma^0 = \frac{\pi\alpha^2}{2s}\sum_{l=1}^{4}M_l^0 + (t \leftrightarrow u) \tag{30}$$

it is easy to make sure that in the IR part of the vertex cross section the Born structure is factorized with t and u terms separated.

C. Boxes

Using the identical transformation, we divide the box cross section into two parts:

$$\sigma^{\mathrm{Box}} = (\sigma^{\mathrm{Box}} - \sigma^{\mathrm{Box}}(\lambda^2 \to s)) + \sigma^{\mathrm{Box}}(\lambda^2 \to s)$$
$$= \sigma_{\mathrm{IR}}^{\mathrm{Box}} + \sigma_{\mathrm{F}}^{\mathrm{Box}}. \tag{31}$$

The IR-finite box cross section looks like

$$\sigma_{\mathrm{F}}^{\mathrm{Box}} = -\frac{\alpha^3}{s}\left(\frac{L_u^2 + \pi^2}{2}\sum_{l=1}^{4}M_l^0 + \sum_{(ij)=1}^{4}\sum_{k=\gamma,Z}B_{(ij)}^k\right) + (t \leftrightarrow u), \tag{32}$$

where $L_u = \log(-s/u)$, the double index (ij) runs like $(ij) = \{1, 2, 3, 4\} = \{\gamma\gamma, \gamma Z, ZZ, WW\}$, and expressions $B_{(ij)}^k$ take the form

$$\begin{aligned}
B_{(\gamma\gamma)}^k &= D^{kt}\lambda_-^{\gamma k}\delta_{(\gamma\gamma)}^1 + (D^{kt} + D^{ku})\lambda_+^{\gamma k}\delta_{(\gamma\gamma)}^2,\\
B_{(\gamma Z)}^k &= D^{kt}\lambda_-^{Zk}\delta_{(\gamma Z)}^1 + (D^{kt} + D^{ku})\lambda_+^{Zk}\delta_{(\gamma Z)}^2,\\
B_{(ZZ)}^k &= D^{kt}\lambda_-^{Bk}\delta_{(ZZ)}^1 + (D^{kt} + D^{ku})\lambda_+^{Bk}\delta_{(ZZ)}^2,\\
B_{(WW)}^k &= D^{kt}\lambda_-^{Ck}\delta_{(WW)}^1 + (D^{kt} + D^{ku})\lambda_+^{Ck}\delta_{(WW)}^2.
\end{aligned} \tag{33}$$

The combinations of the coupling constants are given in (6). Let us recall the coupling constants for ZZ and WW boxes:

$$\begin{aligned}
v^B &= (v^Z)^2 + (a^Z)^2,\\
a^B &= 2v^Z a^Z,\\
v^C &= a^C = 1/(4s_W^2).
\end{aligned} \tag{34}$$

To calculate the corrections $\delta_{(ij)}^{1,2}$ for $(ij) = \{2, 3, 4\}$ we used the low-energy approximation (a detailed example of the low-energy approximation used in the two-boson exchange calculations is presented in Appendix A). Our numerical estimates show the accuracy better than 0.2% in the whole low-energy region $0 < \sqrt{s} < 50$ GeV. The accuracy of the approximate approach improves with the decrease of energy. On the contrary, the calculation of boxes using FEYNARTS and FORMCALC [21] in the region $\sqrt{s} < 1$ GeV suffers from a problem of numerical instability due to Landau singularities. In any case, for the 11 GeV relevant to the JLab experiments, the consistency of calculations for boxes in both approaches is obvious and the discrepancy has an order of $\sim 0.01\%$.

As result, the corrections $\delta_{(ij)}^{1,2}$ have the form:

$$\begin{aligned}
\delta_{(\gamma\gamma)}^1 &= L_s^2(s^2 + u^2)/(2t) - L_s u - (L_x^2 + \pi^2)u^2/t,\\
\delta_{(\gamma\gamma)}^2 &= L_s^2 s^2/t + L_x s - (L_x^2 + \pi^2)(s^2 + u^2)/(2t),
\end{aligned} \tag{35}$$

$$\delta_{(\gamma Z)}^1 = 8u^2(4I_{\gamma Z} - \hat{I}_{\gamma Z}), \qquad \delta_{(\gamma Z)}^2 = 8s^2(I_{\gamma Z} - 4\hat{I}_{\gamma Z}),$$

$$\delta_{(ZZ)}^1 = \frac{3u^2}{2m_Z^2}, \qquad\qquad\qquad \delta_{(ZZ)}^2 = -\frac{3s^2}{2m_Z^2},$$

$$\delta_{(WW)}^1 = \frac{2u^2}{m_W^2}, \qquad\qquad\qquad \delta_{(WW)}^2 = \frac{s^2}{2m_W^2}, \tag{36}$$

where

$$L_s = \log\frac{s}{-t}, \qquad L_x = \log\frac{u}{t}, \tag{37}$$

with

$$I_{\gamma Z} = \frac{1}{2\sqrt{-u}}\int_0^1 z\,dz\int_0^1 dx\,\frac{1}{\sqrt{\beta}}\log\left|\frac{xz\sqrt{-u} - \sqrt{\beta}}{xz\sqrt{-u} + \sqrt{\beta}}\right|, \tag{38}$$

$$\beta = -ux^2z^2 + 4(1-z)(tz(x-1) + m_Z^2),$$

$$\hat{I}_{\gamma Z} = I_{\gamma Z}|_{u \to -s}. \tag{39}$$

Finally, the terms of the box IR cross section $\sigma_{\text{IR}}^{\text{Box}}$ are given by

$$\sigma_{\text{IR}}^{\gamma\gamma\text{-box}} = \frac{\alpha^3}{s} \log\frac{s}{-u} \log\frac{s}{\lambda^2} \sum_{l=1}^{2} M_l^0 + (t \leftrightarrow u), \tag{40}$$

$$\sigma_{\text{IR}}^{\gamma Z\text{-box}} = \frac{\alpha^3}{s} \log\frac{s}{-u} \log\frac{s}{\lambda^2} \sum_{l=3}^{4} M_l^0 + (t \leftrightarrow u), \tag{41}$$

and, summing all the IR terms of the V contribution, we have

$$\sigma_{\text{IR}}^{\text{Ver}} + \sigma_{\text{IR}}^{\text{Box}} = \frac{\alpha^3}{2s}\left(\Lambda_1^{\text{IR}} + 2\log\frac{s}{-u}\log\frac{s}{\lambda^2}\right)$$

$$\times \sum_{l=1}^{4} M_l^0 + (t \leftrightarrow u) = -\frac{\alpha^3}{s}\log\frac{s}{\lambda^2}\log\frac{tu}{em^2s}$$

$$\times \sum_{l=1}^{4} M_l^0 + (t \leftrightarrow u) = -\frac{2\alpha}{\pi}\log\frac{s}{\lambda^2}\log\frac{tu}{em^2s}\sigma^0. \tag{42}$$

IV. BREMSSTRAHLUNG

In order to get the IR-finite result, we have to consider the diagrams with the photon emission (Fig. 3). The whole bremsstrahlung cross section looks like

$$\sigma^R = \frac{\alpha^3}{4s} \int_0^{v^{\text{cut}}} \frac{s-v}{2s} dv \sum_{i,j=\gamma,Z} I[M_R^{ij}], \tag{43}$$

where v^{cut} is the boundary of the region in the Chew-Low diagram [13], and

$$I[M_R^{ij}] = \frac{1}{\pi} \int \frac{d^3k}{k_0} \delta((k_1 + p_1 - k_2 - k)^2 - m^2) M_R^{ij} \tag{44}$$
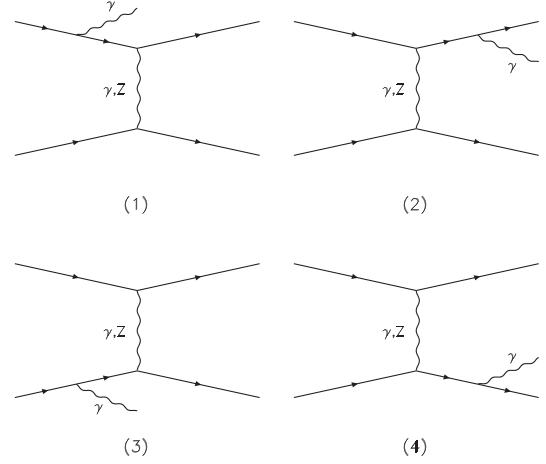

FIG. 3. Bremsstrahlung diagrams for the Møller process in the t channel. The four u-channel diagrams are obtained by means of the interchange $k_2 \leftrightarrow p_2$.

is an integral over phase space of an emitted photon with 4-momentum k. The squared matrix elements corresponding to diagrams in Fig. 3 can be presented as

$$M_R^{ij} = (M_R^{it} - M_R^{iu})(M_R^{jt} - M_R^{ju})^+, \tag{45}$$

where the minus sign is caused by identity of final electrons and the superscripts $t(u)$ denote the $t(u)$-channel diagrams.

Simplifying (45), we have

$$M_R^{it}M_R^{jt+} = \sum_{k=1,4} V_k^{ij}, \qquad M_R^{it}M_R^{ju+} = \sum_{k=5,8} V_k^{ij}, \tag{46}$$

$$M_R^{iu}M_R^{ju+} = M_R^{it}M_R^{jt+}|_{k_2 \leftrightarrow p_2},$$

$$M_R^{iu}M_R^{jt+} = M_R^{it}M_R^{ju+}|_{k_2 \leftrightarrow p_2}, \tag{47}$$

where

$$V_1^{ij} = -\text{Sp}[G_1^{\mu\alpha}\rho^{ij}(k_1)G_1^{\nu\alpha T}\Lambda(k_2)]\text{Sp}[\gamma_\mu\rho^{ij}(p_1)\gamma_\nu\Lambda(p_2)]D^{it_1}D^{jt_1},$$

$$V_2^{ij} = -\text{Sp}[G_1^{\mu\alpha}\rho^{ij}(k_1)\gamma_\nu\Lambda(k_2)]\text{Sp}[\gamma_\mu\rho^{ij}(p_1)G_2^{\nu\alpha T}\Lambda(p_2)]D^{it_1}D^{jt},$$

$$V_3^{ij} = -\text{Sp}[G_2^{\mu\alpha}\rho^{ij}(p_1)\gamma_\nu\Lambda(p_2)]\text{Sp}[\gamma_\mu\rho^{ij}(k_1)G_1^{\nu\alpha T}\Lambda(k_2)]D^{it}D^{jt_1},$$

$$V_4^{ij} = -\text{Sp}[G_2^{\mu\alpha}\rho^{ij}(p_1)G_2^{\nu\alpha T}\Lambda(p_2)]\text{Sp}[\gamma_\mu\rho^{ij}(k_1)\gamma_\nu\Lambda(k_2)]D^{it}D^{jt},$$

$$V_5^{ij} = -\text{Sp}[G_1^{\mu\alpha}\rho^{ij}(k_1)G_3^{\nu\alpha}\Lambda(p_2)\gamma_\mu\rho^{ij}(p_1)\gamma_\nu\Lambda(k_2)]D^{it_1}D^{ju},$$

$$V_6^{ij} = -\text{Sp}[G_1^{\mu\alpha}\rho^{ij}(k_1)\gamma_\nu\Lambda(p_2)\gamma_\mu\rho^{ij}(p_1)G_4^{\nu\alpha}\Lambda(k_2)]D^{it_1}D^{jz_2},$$

$$V_7^{ij} = -\text{Sp}[\gamma_\mu\rho^{ij}(k_1)G_3^{\nu\alpha}\Lambda(p_2)G_2^{\mu\alpha}\rho^{ij}(p_1)\gamma_\nu\Lambda(k_2)]D^{it}D^{ju},$$

$$V_8^{ij} = -\text{Sp}[\gamma_\mu\rho^{ij}(k_1)\gamma_\nu\Lambda(p_2)G_2^{\mu\alpha}\rho^{ij}(p_1)G_4^{\nu\alpha}\Lambda(k_2)]D^{it}D^{jz_2}. \tag{48}$$

We used the radiative invariants which are zero at $k \to 0$:

$$z_1 = 2kk_1, \qquad z = 2kk_2, \qquad v_1 = 2kp_1,$$
$$v = 2kp_2 = s + u + t - 4m^2, \qquad (49)$$

and the invariants for propagator structure as

$$t_1 = (p_1 - p_2)^2, \qquad z_2 = (k_1 - p_2)^2. \qquad (50)$$

Also, we applied a short abbreviation for combinations with $\rho(p)$, the density matrix of a particle with 4-momentum p, defined as

$$\rho^{ij}(p) = (v^i - a^i \gamma_5)\rho(p)(v^j + a^j \gamma_5)$$
$$= \tfrac{1}{2}(\lambda_{1B}^{ij}\hat{p} - \lambda_{2B}^{ij}\gamma_5\hat{p}) + \mathcal{O}(m). \qquad (51)$$

We define

$$\Lambda(p) = \hat{p} + m, \qquad \hat{p} = \gamma^\mu p_\mu, \qquad (52)$$

and

$$G_1^{\mu\alpha} = \gamma^\mu \frac{2k_1^\alpha - \hat{k}\gamma^\alpha}{-z_1} + \frac{2k_2^\alpha + \gamma^\alpha\hat{k}}{z}\gamma^\mu,$$

$$G_2^{\mu\alpha} = \gamma^\mu \frac{2p_1^\alpha - \hat{k}\gamma^\alpha}{-v_1} + \frac{2p_2^\alpha + \gamma^\alpha\hat{k}}{v}\gamma^\mu,$$

$$G_3^{\nu\alpha} = \frac{2k_1^\alpha - \gamma^\alpha\hat{k}}{-z_1}\gamma^\nu + \gamma^\nu \frac{2p_2^\alpha + \hat{k}\gamma^\alpha}{v},$$

$$G_4^{\nu\alpha} = \frac{2p_1^\alpha - \gamma^\alpha\hat{k}}{-v_1}\gamma^\nu + \gamma^\nu \frac{2k_2^\alpha + \hat{k}\gamma^\alpha}{z}.$$

The bremsstrahlung cross section can be broken down into two parts (soft and hard) as

$$\sigma^R = \sigma_{IR}^R + \sigma_H^R \qquad (53)$$

by separating the integration domain according to $k_0 < \omega$ or $k_0 > \omega$, where k_0 is the photon energy (in the reference frame comoving with the center of mass of the primary electrons) and ω is a parameter corresponding to the maximum soft photon energy. The easiest way to implement such a partition is to multiply the integrand in (43) by $\theta(\omega - k_0)$ and neglect photon momentum $k \to 0$ where possible, which would give us the soft photon cross section.

A. Soft photons and IR-divergence cancellation

First, we follow the methods of paper [26] to get a well-known result (see also [11,12]) for the soft photon cross section:

$$\sigma_{IR}^R = \frac{\alpha}{\pi}\left(4\log\frac{2\omega}{\lambda}\log\frac{tu}{em^2 s} - \log^2\frac{s}{em^2} + 1 - \frac{\pi^2}{3}\right.$$
$$\left. + \log^2\frac{u}{t}\right)\sigma^0. \qquad (54)$$

Next, we sum the IR terms of V and R contributions [Eqs. (42) and (54)],

$$\sigma^C = \sigma_{IR}^V + \sigma_{IR}^R$$
$$= \frac{\alpha}{\pi}\left(2\log\frac{4\omega^2}{s}\log\frac{tu}{em^2 s} - \log^2\frac{s}{em^2} + 1 - \frac{\pi^2}{3}\right.$$
$$\left. + \log^2\frac{u}{t}\right)\sigma^0 \qquad (55)$$

and get a result free from IR divergence which logarithmically depends on ω and contains $\log^2(s/m^2)$ terms. Adding the contribution corresponding to Λ_1 to σ^C, we get an expression with the first power of collinear logarithms:

$$\sigma^{Ver} + \sigma^C \sim \frac{\alpha}{\pi}\left(\Lambda_1(\lambda^2 \to s) - \log^2\frac{s}{m^2}\right) + \cdots$$
$$= \frac{\alpha}{\pi}\left(\log^2\frac{-t}{m^2} - \log^2\frac{s}{m^2}\right) + \cdots$$
$$= \frac{\alpha}{\pi}\log\frac{-t}{s}\log\frac{-ts}{m^4} + \cdots \qquad (56)$$

with nonphysical dependences canceled analytically.

B. Hard photons: Leading logarithms approach

Now we will calculate the HPB cross section retaining in the result the leading collinear logarithms. This approach allows estimating the EWC very rapidly yet provides a rather accurate result. First let us consider exact collinear kinematics, with all relevant information given in Table II of Appendix B. As one can see from this table, $z + v \approx (1 - \eta)s$ for all peaks. Using the radiative invariants $k_0 = (v + z)/(2\sqrt{s})$, we can transform the region of integration over v into

$$1 - 2\frac{\Omega}{\sqrt{s}} < \eta < 1 - 2\frac{\omega}{\sqrt{s}}, \qquad (57)$$

where Ω is the maximal energy of the emitted hard photon.

Now, integrating over photon phase space and taking into consideration the results from Table II of Appendix B to simplify, we get the hard part of the bremsstrahlung cross section as

$$\sigma_H^R = \frac{\alpha^3}{4s}\int_{1-2\Omega/\sqrt{s}}^{1-2\omega/\sqrt{s}} \frac{d\eta}{1-\eta}h(\eta), \qquad (58)$$

where

$$h(\eta) = h_{ev,t}(\eta) + h_{od,t}(\eta) + (k_2 \leftrightarrow p_2), \qquad (59)$$

and

$$h_{\mathrm{ev,t}}(\eta) = \frac{s-v}{s}\left(\left(2l_m - 2 + \frac{(1-\eta)^2}{\eta}\hat{l}_a\right)\sum_{i,j=\gamma,Z} M_{\mathrm{ev}}^{ijij}(\eta s, u)D^{it_1}D^{jt_1}|^{z_1} + \left(2l_m - 2 + \frac{(1-\eta)^2}{\eta}l_a\right)\right.$$

$$\times \sum_{i,j=\gamma,Z} M_{\mathrm{ev}}^{ijij}(s, u/\eta)D^{it_1}D^{jt_1}|^z + (\hat{l}_a - l_s)\sum_{i,j=\gamma,Z} M_{\mathrm{ev}}^{ijij}(\eta s, u)(D^{it_1}D^{jt} + D^{it}D^{jt_1})|^{z_1} + (l_x - l_a)$$

$$\times \sum_{i,j=\gamma,Z} M_{\mathrm{ev}}^{ijij}(s, u/\eta)(D^{it_1}D^{jt} + D^{it}D^{jt_1})|^z + ((1-\eta)^2 l_u - 2\eta)\sum_{i,j=\gamma,Z} M_{\mathrm{ev}}^{ijij}(s, u)D^{it}D^{jt}|^{v_1}$$

$$\left. + 2\left(\frac{(1-\eta)^2 - \eta}{2-\eta} + \eta l_u\right)\sum_{i,j=\gamma,Z} M_{\mathrm{ev}}^{ijij}(s, u)D^{it}D^{jt}|^v\right),$$

$$h_{\mathrm{od,t}}(\eta) = \frac{v-s}{s}\sum_{i,j=\gamma,Z} M_{\mathrm{od}}^{ijij}\left((\eta(\eta^2 - \eta + 1)\hat{l}_a + \eta^2 l_m - 2\eta^2)D^{it_1}D^{ju}|^{z_1} + (l_m - l_a)D^{it_1}D^{ju}|^z + \eta^2(l_m - l_s)D^{it_1}D^{jz_2}|^{z_1}\right.$$

$$+ \left(l_x + l_m + \frac{(1-\eta)^2}{\eta}l_a - 2\right)D^{it_1}D^{jz_2}|^z + \eta^2(\hat{l}_a - l_s)D^{it}D^{ju}|^{z_1} + \left(l_u - \frac{2}{\eta}\right)D^{it}D^{ju}|^v$$

$$\left. + ((\eta^2 - \eta + 1)l_u - 2\eta)D^{it}D^{jz_2}|^{v_1} + (l_x - l_a)D^{it}D^{jz_2}|^z\right). \tag{60}$$

The logarithms above look like

$$l_a = \log\frac{(s-v)^2}{m^2\tau}, \qquad \hat{l}_a = \log\frac{(s+t)^2}{m^2\tau},$$

$$l_m = \log\frac{-t}{m^2}, \qquad l_s = \log\frac{s^2}{m^4}, \tag{61}$$

$$l_u = \log\frac{(s+u)^2}{m^2\tau}, \qquad l_x = \log\frac{u^2}{m^4}$$

with $\tau = v + m^2$. An operation $E|^x$ denotes the calculation of an E expression in the x peak.

Using the standard designation of the IR-divergence extracting operation (see pioneer paper [27])

$$\int \frac{d\eta}{(1-\eta)_+}f(\eta) = \int \frac{d\eta}{1-\eta}(f(\eta) - f(1)) \tag{62}$$

we can present the hard part as

$$\sigma_H^R = \sigma_H^{R,\Omega} + \sigma_H^{R,\omega}$$

$$= \frac{\alpha^3}{4s}\int_{1-2(\Omega/\sqrt{s})}^{1-2(\omega/\sqrt{s})}\frac{d\eta}{(1-\eta)_+}h(\eta)$$

$$+ \frac{\alpha^3}{4s}\int_{1-2(\Omega/\sqrt{s})}^{1-2(\omega/\sqrt{s})}\frac{d\eta}{1-\eta}h(1). \tag{63}$$

Obviously, the first term in (63) is independent of ω (at sufficiently small ω it depends on Ω only), and the second term can be easily calculated as

$$\sigma_H^{R,\omega} = \frac{\alpha^3}{4s}h(1)\int_{1-2(\Omega/\sqrt{s})}^{1-2(\omega/\sqrt{s})}\frac{d\eta}{1-\eta}$$

$$= \frac{4\alpha}{\pi}\log\frac{\Omega}{\omega}\log\frac{tu}{em^2s}\sigma^0. \tag{64}$$

Finally, we obtain the desired result where the sum of all contributions to lowest order radiative corrections is independent of ω:

$$\sigma_C + \sigma_H^{R,\omega} = \sigma_C(\omega \to \Omega). \tag{65}$$

V. NUMERICAL ANALYSIS

Figure 4 shows the Born asymmetry A_1^0 versus θ at the energy of the previous JLab experiment at $E_{\mathrm{lab}} = 3.03$ GeV (solid line) and the energy of the planned one with $E_{\mathrm{lab}} = 11$ GeV (dashed line). Here, we used $\alpha = 1/137.035\,999$, $m_W = 80.398$ GeV, and $m_Z = 91.1876$ GeV according
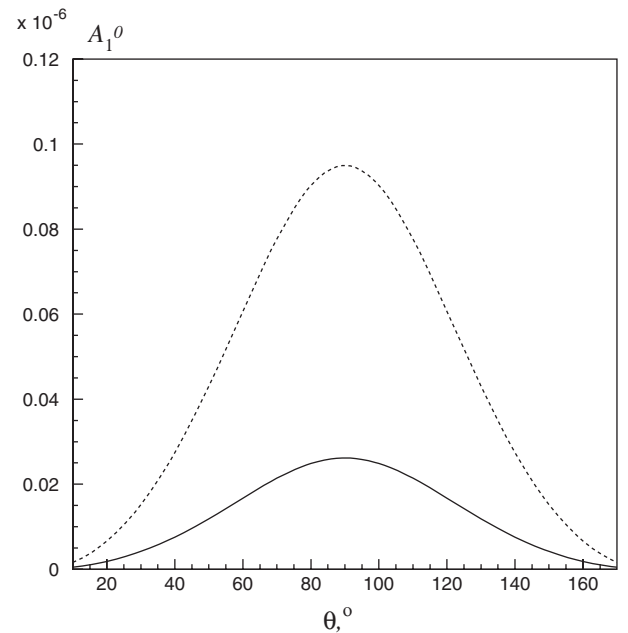

FIG. 4. Born asymmetry versus θ at $E_{\mathrm{lab}} = 3.03$ GeV (solid line), 11 GeV (dashed line).

to [28]. It is clear that at low energies the asymmetry A_1^0 is proportional to $s = 2mE_{lab}$ giving $A_1^0(11\ \text{GeV})/A_1^0(3.03\ \text{GeV}) \approx 4$ for any θ.

For the detailed numerical calculation of EWC, we take the electron, muon, and τ-lepton masses as $m_e = 0.510\,998\,910$ MeV, $m_\mu = 0.105\,658\,367$ GeV, $m_\tau = 1.776\,84$ GeV and the quark masses for loop contributions as $m_u = 0.069\,83$ GeV, $m_c = 1.2$ GeV, $m_t = 174$ GeV, $m_d = 0.069\,84$ GeV, $m_s = 0.15$ GeV, and $m_b = 4.6$ GeV. The light quark masses provide $\Delta\alpha_{had}^{(5)}(m_Z^2) = 0.027\,57$ [29], where

$$\Delta\alpha_{had}^{(5)}(s) = \frac{\alpha}{\pi} \sum_{f=u,d,s,c,b} Q_f^2 \left(\log\frac{s}{m_f^2} - \frac{5}{3}\right), \quad (66)$$

Q_f is the electric charge of fermion f in proton charge units q ($q = \sqrt{4\pi\alpha}$). We believe that the use of the light quark masses as parameters regulated by the hadron vacuum polarization is a better choice in this case. Finally, for the mass of the Higgs boson, we take $m_H = 115$ GeV. Although this mass is still to be determined experimentally, the dependence of EWC on m_H is rather weak.

Let us define the relative corrections to the Born cross section as

$$\delta^C = (\sigma^C - \sigma^0)/\sigma^0, \qquad C = \text{BSE, Ver, Box, ...}$$

and to the Born asymmetry as

$$\delta_A^C = (A_1^C - A_1^0)/A_1^0.$$

For convenience, we define *weak* for relative corrections as all BSE contributions (including $\gamma\gamma$-SE which is not weak by nature, but we need it here to account for all the IR-finite contributions to the asymmetry), HV, ZZ and WW boxes. This way, $weak = \text{BSE} + \text{HV} + ZZ + WW$.

We present all weak and total (total = weak + QED) relative corrections to the unpolarized cross section at $E_{lab} = 11$ GeV and different angles θ with different cuts on soft ("S") and hard ("S + H") photon emission energy given by various γ_1 ($\gamma_1 = E_\gamma/\sqrt{s}$) in Table III of Appendix C. Empty cells correspond to forbidden kinematical regions of this process. If $E_\gamma = \omega$, we take into consideration only soft photons and if $E_\gamma = \Omega$, both soft and hard photons are taken into account. In principle, for $E_\gamma = \Omega$, we should treat $\omega/\sqrt{s}$ as a small parameter but, as it was shown in Eq. (65), the total result does not depend on it in any case. The $\gamma\gamma$-SE contribution is small but still dominates the relative weak correction to the unpolarized cross section. We can also see a rather small difference between contributions S and S + H. Additionally, we can conclude that the unpolarized cross section significantly drops with the decrease of γ_1.

All weak and QED relative corrections to the asymmetry A_1^0 at $E_{lab} = 11$ GeV are presented in Tables IV and V in Appendix C. At $\theta = 90°$ the $\gamma\gamma$-SE gives ~ -0.007 to the relative weak correction, the γZ-SE gives a consider-

able contribution and the ZZ-SE gives a contribution which is nonzero but not as large as that from γZ-SE. It is unphysical to separate the BSE and HV due to the fact that only their sum gives a gauge invariant set. We show their contribution as a total weak correction in Table IV. The WW boxes give a rather significant input: $\delta_A^{WW} = 0.0238$, but the result coming from the ZZ boxes is rather small and equal to $\delta_A^{ZZ} = -0.0013$. Finally, we can see from Table V that the total relative QED corrections are significant and strongly depend on the parameter γ_1.

At this point, it is essential to compare the corrected parity-violating asymmetry, which is sensitive to input parameters and calculation scheme, with well-known existing results. In Fig. 5 we can see the relative weak (solid line) and QED including soft (dashed line) corrections to the Born asymmetry A_1^0 versus $\sqrt{s}$ at $\theta = 90°$. In the region of high energies ($\sqrt{s} \gtrsim 50$ GeV) we can see an excellent agreement with the result of Denner and Pozzorini [11] if we use their standard model parameters (see Table I for δ_A^{weak} at different $\sqrt{s}$).

Furthermore, the relative QED corrections (see Fig. 8 in Ref. [11] and dashed line in Fig. 5 here) are also in good qualitative and numerical agreement. In this case, we apply the same cut on the soft photon emission energy as in Ref. [11] ($\gamma_1 = 0.05$).

In our calculations we chose to use the set of input parameters α, m_W, and m_Z since m_W has a well-defined value with constantly increasing accuracy. The set of input parameters consisting of α, the Fermi constant G_F, and m_Z was popular when the W-boson mass was not as well
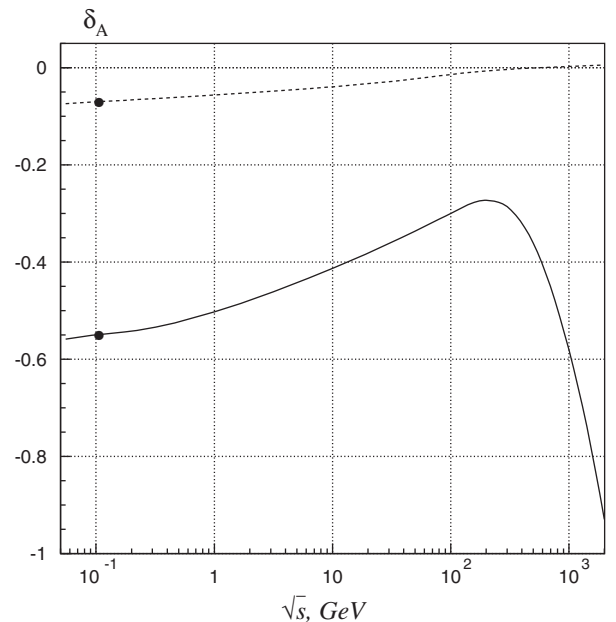

FIG. 5. The relative weak (solid line) and QED (dashed line) corrections to the Born asymmetry A_1^0 versus $\sqrt{s}$ at $\theta = 90°$. The filled circle corresponds to our predictions of the future 11 GeV Møller experiment at JLab.

TABLE I.   Comparison of our result for δ_A^{weak} with the result of [11].

$\sqrt{s}$, GeV	Result of Ref. [11]	Our result
100	−0.2787	−0.2790
500	−0.3407	−0.3406
2000	−0.9056	−0.9066

known (see papers [30,31], for example). However, this set was used successfully for the calculation of radiative corrections for several modern experiments including the recent experiment E-158 [10]. At kinematics of the E-158 and using our parameter set we find that $\delta_A^{\text{weak}} \approx -54\%$. For comparison purposes, if we express our input parameters in terms of α, G_F, and m_Z, we obtain a good agreement with the result of [10].

VI. CONCLUSION

Møller scattering is a very clean process that can provide indirect access to new physics at multi-TeV scales. The new ultraprecise measurement of the weak mixing angle via 11 GeV Møller scattering starting soon at JLab will require the higher order effects to be taken into account with the highest precision as well. In this work, we calculate the electroweak radiative corrections to the asymmetry of polarized Møller scattering at energies relevant to the future experiments at JLab. The results are presented in both numerical and analytical form. As one can clearly see from our numerical data, at certain kinematic conditions EWC can reduce the asymmetry up to ~70%, and they depend quite strongly on the experimental cuts. In the on-shell renormalization scheme we use, the largest contribution is coming from the weak corrections: self-energy graphs (especially γZ-SE), HV, and boxes. The QED part is obviously very important as well.

We believe that one of the most important results of this work, however, is our compact analytical and sufficiently accurate expressions. They can be useful for fast yet relatively precise estimations and are well suitable for building Monte Carlo generators. Our final results are analytically free from any nonphysical parameters. The accuracy was controlled by comparison with the numerical data obtained by a semiautomatic approach using FEYNARTS and FORMCALC. These base languages were already successfully employed in similar projects (see [32,33], for example), so we are highly confident in their reliability.

Since the problem of EWC for Møller scattering is rather involved, we believe that a tuned step-by-step comparison between different calculation approaches is essential. In the next work, we plan to present a detailed comparison between several calculation approaches with different renormalization schemes. We also plan to address the leading two-loop electroweak corrections which are very likely to be required by the promised experimental precision. To maximize the precision, the full set of one-loop EWC evaluated in this paper will also need to be recalculated with the latest input parameters available at the time of completion of the measurements, but this will be easy to do based on the results of the present work.

ACKNOWLEDGMENTS

APPENDIX A: A DETAILED EXAMPLE OF THE LOW-ENERGY APPROXIMATION IN TWO-BOSON EXCHANGE CALCULATIONS

In order to provide simplified expressions for quick and reliable estimates, we evaluate box diagrams with two massive boson exchanges by extracting the leading part in the low-energy region. As an example, we show here detailed calculations for the part of the cross section corresponding to a product of a t-channel crossed ZZ box and Hermitian-conjugate Born matrix element (Fig. 6). The other parts of the cross section are easy to get (a) by replacement of indices ($Z \to W$) to obtain a WW box, (b) switching momentum transfer labels in a diagram to get the direct box, and (c) exchanging t and u ($t \leftrightarrow u$) to arrive at an expression for the u channel. Since for Møller scattering the direct WW boxes are forbidden by the charge conservation law, we are left with a crossed-box diagram for the case of the charged current reaction. The part of the cross section corresponding to Fig. 6 is calculated in the ultrarelativistic approximation and has the following form:

$$\sigma^{ZZ\text{-crossed}} = -\frac{\alpha^3}{s} \sum_{k=\gamma,Z} D^{kt} \frac{i}{(2\pi)^2} \int d^4k \frac{\text{Sp}[\gamma^\alpha \hat{p}_2 \gamma_\nu (\hat{p}_2 - \hat{k})\gamma_\mu \rho^{Bk}(p_1)]\text{Sp}[\gamma_\alpha \hat{k}_2 \gamma^\mu (\hat{k}_1 - \hat{k})\gamma^\nu \rho^{Bk}(k_1)]}{(k^2 - 2k_1k)(k^2 - 2p_2k)(k^2 - m_Z^2)((k-q)^2 - m_Z^2)}. \tag{A1}$$

Next, we need to evaluate the following scalar, vector, and tensor integrals:

$$I_{(0,\nu,\mu\nu)}^{ZZ} = \frac{i}{(2\pi)^2} \int \frac{(1, k_\nu, k_\mu k_\nu)d^4k}{(k^2 - 2k_1k)(k^2 - 2p_2k)(k^2 - m_Z^2)((k-q)^2 - m_Z^2)}. \tag{A2}$$
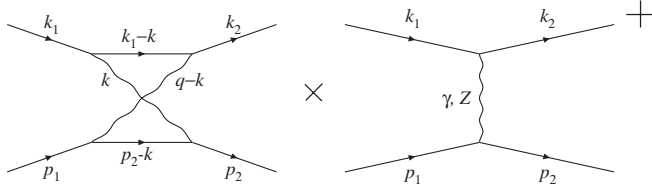
FIG. 6. Example of an interference term coming from the *t*-channel crossed ZZ box and Hermitian conjugated Born contribution, to illustrate the low-energy approximation in two-boson exchange calculations.

Applying the Feynman parametrization [34], we obtain

$$I^{ZZ}_{(0,\nu,\mu\nu)} = \frac{i}{(2\pi)^2} 3! \int_0^1 z^2 dz \int_0^1 x dx \int_0^1 dy$$
$$\times \int \frac{(1, k_\nu, k_\mu k_\nu) d^4 k}{[k^2 - 2kp + \Delta]^4}, \quad (A3)$$

where

$$p = q(1 - z) + k_1 xyz + p_2 xz(1 - y),$$
$$\Delta = q^2(1 - z) + m_Z^2(xz - 1). \quad (A4)$$

Taking the integral over k using well-known expressions (see [35], for example), we obtain

$$I^{ZZ}_{(0,\nu,\mu\nu)} = -\frac{1}{4} \int_0^1 z^2 dz \int_0^1 x dx \int_0^1 dy$$
$$\times \frac{(1, p_\nu, p_\mu p_\nu - g_{\mu\nu}(p^2 - \Delta)/2)}{[p^2 - \Delta]^2}. \quad (A5)$$

Since Δ clearly gives a dominant contribution, it is now easy to arrive at the approximate expression in the low-energy area we are interested in $(s, |t|, |u| \ll m_Z^2)$. Then, for example:

$$I^{ZZ}_{\mu\nu} \approx \frac{g_{\mu\nu}}{8} \int_0^1 z^2 dz \int_0^1 x dx \int_0^1 dy \frac{1}{p^2 - \Delta}$$
$$\approx -\frac{g_{\mu\nu}}{8m_Z^2} \int_0^1 z^2 dz \int_0^1 x dx \int_0^1 dy \frac{1}{xz - 1}$$
$$= -\frac{g_{\mu\nu}}{8m_Z^2} \int_0^1 dz \int_{x=0}^{x=1} d(xz) \frac{xz}{xz - 1}$$
$$= -\frac{g_{\mu\nu}}{8m_Z^2} \int_0^1 dz(z + \ln|1 - z|) = \frac{g_{\mu\nu}}{16m_Z^2}. \quad (A6)$$

This outlines the technique we used to obtain the compact expressions (36).

APPENDIX B: COLLINEAR KINEMATICS

TABLE II.   Kinematic relationships relevant to the hard photon cross section.

	z_1 peak	z peak	v_1 peak	v peak
k	$(1 - \eta)k_1$	$\frac{1-\eta}{\eta} k_2$	$(1 - \eta)p_1$	$\frac{1-\eta}{\eta} p_2$
z_1	$2(1 - \eta)m^2 \to 0$	$\frac{1-\eta}{\eta}(2m^2 - t)$	$(1 - \eta)(s - 2m^2)$	$(1 - \eta)(s + t - 4m^2 + \frac{2m^2}{\eta})$
z	$(1 - \eta)(2m^2 - t)$	$2\frac{1-\eta}{\eta} m^2 \to 0$	$\frac{1-\eta}{\eta}(\eta s + t - 2m^2)$	$(1 - \eta)(s - 2m^2)$
v_1	$(1 - \eta)(s - 2m^2)$	$\frac{1-\eta}{\eta}(\eta(s - 2m^2) + t)$	$2(1 - \eta)m^2 \to 0$	$(1 - \eta)(2m^2 - t)$
v	$(1 - \eta)(s + t - 2m^2)$	$(1 - \eta)(s - 2m^2)$	$\frac{1-\eta}{\eta}(2m^2 - t)$	$2\frac{1-\eta}{\eta} m^2 \to 0$
u	$\eta(2m^2 - s - t) + 2m^2$	$2m^2 - t - \eta(s - 2m^2)$	$2m^2 - s + \frac{2m^2 - t}{\eta}$	$2m^2 - s - t + \frac{2m^2}{\eta}$
$k_2 p_2$	$\eta \cdot k_1 p_1$	$\eta \cdot k_1 p_1$	$\eta \cdot k_1 p_1$	$\eta \cdot k_1 p_1$
$p_1 p_2$	$\eta \cdot k_1 k_2$	$\frac{1}{\eta} \cdot k_1 k_2$	$\frac{1}{\eta} \cdot k_1 k_2$	$\eta \cdot k_1 k_2$
$k_1 p_2$	$\frac{1}{\eta} \cdot p_1 k_2$	$\frac{1}{\eta} \cdot p_1 k_2$	$\eta \cdot p_1 k_2$	$\eta \cdot p_1 k_2$

APPENDIX C: NUMERICAL ANALYSIS

TABLE III.   The unpolarized Born cross section and the relative *weak* and total corrections to it at $E_{lab} = 11$ GeV at different γ_1 ($\gamma_1 = 0.005, 0.01, 0.05$) and θ.

$\theta,°$	σ^0, mb	Weak	S, 0.005	S + H, 0.005	S, 0.01	S + H, 0.01	S, 0.05	S + H, 0.05
20	0.1277×10^2	0.0087	−0.2149	−0.2148	−0.1754	−0.1758	⋯	⋯
30	0.2607×10^1	0.0101	−0.2417	−0.2415	−0.1972	−0.1978	⋯	⋯
40	0.8734	0.0111	−0.2595	−0.2591	−0.2118	−0.2124	−0.1012	−0.1067
50	0.3920	0.0119	−0.2721	−0.2716	−0.2222	−0.2227	−0.1063	−0.1136
60	0.2176	0.0126	−0.2810	−0.2805	−0.2295	−0.2303	−0.1099	−0.1183
70	0.1444	0.0131	−0.2870	−0.2867	−0.2344	−0.2356	−0.1124	−0.1219
80	0.1131	0.0135	−0.2905	−0.2904	−0.2373	−0.2389	−0.1139	−0.1241
90	0.1043	0.0136	−0.2916	−0.2916	−0.2383	−0.2400	−0.1144	−0.1249

TABLE IV.   The Born asymmetry A_1^0 and the structure of relative weak corrections to it at $E_{lab} = 11$ GeV at different θ.

$\theta,°$	A_1^0, ppb	$\gamma\gamma$-SE	γZ-SE	ZZ-SE	All BSE	ZZ box	WW box	HV	Weak
20	6.63	−0.0043	−0.2919	−0.0105	−0.2863	−0.0013	0.0239	−0.2946	−0.5643
30	15.19	−0.0049	−0.2916	−0.0105	−0.3065	−0.0013	0.0238	−0.2633	−0.5430
40	27.45	−0.0054	−0.2914	−0.0105	−0.3051	−0.0013	0.0238	−0.2727	−0.5508
50	43.05	−0.0058	−0.2912	−0.0105	−0.3042	−0.0013	0.0239	−0.2703	−0.5489
60	60.69	−0.0062	−0.2911	−0.0105	−0.3045	−0.0013	0.0239	−0.2714	−0.5500
70	77.68	−0.0064	−0.2910	−0.0105	−0.3040	−0.0013	0.0238	−0.2712	−0.5495
80	90.28	−0.0066	−0.2909	−0.0105	−0.3040	−0.0013	0.0238	−0.2711	−0.5493
90	94.97	−0.0067	−0.2909	−0.0105	−0.3043	−0.0013	0.0238	−0.2710	−0.5493

TABLE V.   The Born asymmetry and the QED corrections to it at $E_{lab} = 11$ GeV at different γ_1 ($\gamma_1 = 0.005, 0.01, 0.05$) and θ.

$\theta,°$	A_1^0, ppb	S, 0.005	S + H, 0.005	S, 0.01	S + H, 0.01	S, 0.05	S + H, 0.05
20	6.63	−0.0710	−0.0649	−0.0676	−0.0566	$\cdots$	$\cdots$
30	15.19	−0.0758	−0.0736	−0.0716	−0.0686	$\cdots$	$\cdots$
40	27.45	−0.0792	−0.0790	−0.0744	−0.0744	−0.0651	−0.0567
50	43.05	−0.0817	−0.0826	−0.0763	−0.0778	−0.0663	−0.0660
60	60.69	−0.0833	−0.0843	−0.0777	−0.0797	−0.0671	−0.0691
70	77.68	−0.0844	−0.0859	−0.0785	−0.0805	−0.0675	−0.0701
80	90.28	−0.0849	−0.0863	−0.0789	−0.0806	−0.0677	−0.0702
90	94.97	−0.0850	−0.0863	−0.0790	−0.0806	−0.0678	−0.0702

[1] M. Swartz *et al.*, Nucl. Instrum. Methods Phys. Res., Sect. A **363**, 526 (1995).

[2] P. Steiner *et al.*, Nucl. Instrum. Methods Phys. Res., Sect. A **419**, 105 (1998).

[3] H. Band *et al.*, Nucl. Instrum. Methods Phys. Res., Sect. A **400**, 24 (1997).

[4] M. Hauger *et al.*, Nucl. Instrum. Methods Phys. Res., Sect. A **462**, 382 (2001).

[5] J. Arrington *et al.*, Nucl. Instrum. Methods Phys. Res., Sect. A **311**, 39 (1992).

[6] G. Alexander and I. Cohen, Nucl. Instrum. Methods Phys. Res., Sect. A **486**, 552 (2002).

[7] K. S. Kumar *et al.*, Mod. Phys. Lett. A **10**, 2979 (1995); Eur. Phys. J. A **32**, 531 (2007); P. L. Anthony *et al.* (SLAC E158 Collaboration), Phys. Rev. Lett. **92**, 181602 (2004).

[8] J. Benesch *et al.*, www.jlab.org/~armd/moller_proposal.pdf, 2008.

[9] C. A. Heusch, Int. J. Mod. Phys. A **15**, 2347 (2000); J. L. Feng, Int. J. Mod. Phys. A **15**, 2355 (2000).

[10] A. Czarnecki and W. Marciano, Phys. Rev. D **53**, 1066 (1996).

[11] A. Denner and S. Pozzorini, Eur. Phys. J. C **7**, 185 (1999).

[12] F. J. Petriello, Phys. Rev. D **67**, 033006 (2003).

[13] V. A. Zykunov, Yad. Fiz. **67**, 1366 (2004) [Phys. At. Nucl. **67**, 1342 (2004)].

[14] Yu. Kolomensky *et al.*, Int. J. Mod. Phys. A **20**, 7365 (2005).

[15] V. A. Zykunov *et al.*, SLAC-PUB-11378, 2005 [arXiv: hep-ph/0507287].

[16] D. Yu. Bardin and N. M. Shumeiko, Nucl. Phys. **B127**, 242 (1977); Sov. J. Nucl. Phys. **29**, 969 (1979).

[17] N. M. Shumeiko and J. G. Suarez, J. Phys. G **26**, 113 (2000).

[18] A. N. Ilyichev and V. A. Zykunov, Phys. Rev. D **72**, 033018 (2005).

[19] A. Afanasev, Eu. Chudakov, A. Ilyichev, and V. Zykunov, Comput. Phys. Commun. **176**, 218 (2007).

[20] V. A. Zykunov, Yad. Fiz. **72**, 1540 (2009) [Phys. At. Nucl. **72**, 1486 (2009)].

[21] T. Hahn and M. Perez-Victoria, Comput. Phys. Commun. **118**, 153 (1999).

[22] I. V. Akushevich and N. M. Shumeiko, J. Phys. G **20**, 513 (1994).

[23] F. Cuypers and P. Gambino, Phys. Lett. B **388**, 211 (1996).

[24] M. Böhm, H. Spiesberger, and W. Hollik, Fortschr. Phys. **34**, 687 (1986).

[25] A. Denner, Fortschr. Phys. **41**, 307 (1993).

[26] G. 't Hooft and M. Veltman, Nucl. Phys. **B153**, 365 (1979).

[27] G. Altarelli and G. Parisi, Nucl. Phys. **B126**, 298 (1977).

[28] C. Amsler *et al.*, Phys. Lett. B **667**, 1 (2008).

[29] F. Jegerlehner, J. Phys. G **29**, 101 (2003).

[30] W. J. Marciano and A. I. Sanda, Phys. Rev. D **17**, 3055 (1978); Phys. Lett. **77B**, 383 (1978); E. Derman and W. J. Marciano, Ann. Phys. (N.Y.) **121**, 147 (1979).

[31] R. Cahn and G. Kane, Phys. Lett. **71B**, 348 (1977).

[32] A. Aleksejevs *et al.*, J. Phys. G **36**, 045101 (2009).

[33] A. Aleksejevs *et al.*, Yad. Fiz. **73**, 2077 (2010) [Phys. At. Nucl. **73**, 2022 (2010)].

[34] R. Feynman, Phys. Rev. **76**, 769 (1949).

[35] J. Kahane, Phys. Rev. **135**, B975 (1964).